CrystEngComm

PAPER

View Article Online
View Journal | View Issue

Cite this: *CrystEngComm*, 2017, **19**, 4201

Fe_3O_4@HKUST-1 and Pd/Fe_3O_4@HKUST-1 as magnetically recyclable catalysts prepared *via* conversion from a Cu-based ceramic†

Takashi Toyao, [ab] Mark J. Styles,[c] Tokuichiro Yago,[a] Muhammad M. Sadiq, [d] Raffaele Riccò, [ce] Kiyonori Suzuki,[d] Yu Horiuchi,[a] Masahide Takahashi, [a] Masaya Matsuoka*[a] and Paolo Falcaro *[ce]

Received 24th February 2017,
Accepted 22nd May 2017

DOI: 10.1039/c7ce00390k

rsc.li/crystengcomm

Nanocomposites obtained by integrating iron oxide magnetic nanoparticles (Fe_3O_4) into a metal–organic framework (HKUST-1 or $Cu_3(BTC)_2$, BTC = 1,3,5-benzenetricarboxylate) are synthesized through conversion from a composite of a Cu-based ceramic material and Fe_3O_4. *In situ* small-angle X-ray scattering (SAXS) and wide-angle X-ray scattering (WAXS) measurements reveal that the presence of Fe_3O_4 leads to the fast conversion and synthesis of HKUST-1 with small particle sizes. The prepared MOF composite (Fe_3O_4@HKUST-1) is found to catalyze the one-pot sequential deacetalization–Knoevenagel condensation reaction as a magnetically collectable and recyclable catalyst. In addition, Pd nanoparticles are also incorporated into the material (Pd/Fe_3O_4@HKUST-1) by addition of a Pd colloidal solution during the conversion of the precursor composite to HKUST-1. The resulting Pd/Fe_3O_4@HKUST-1 can be utilized for hydrogenation of 1-octene in the liquid phase.

Introduction

Metal–organic frameworks (MOFs), also called porous coordination polymers (PCPs), are a class of crystalline hybrid materials prepared *via* well-established principles of coordination chemistry using self-assembly of metal ions or metal clusters with organic linkers.[1–3] Unlike traditional inorganic porous materials, unlimited possible combinations of such an assembly enables access to reticular structures with tunable porosity and attractive functionalities.[4–7] In addition, new synergetic properties have been obtained by incorporating functional species into MOFs, further expanding their potential applications.[8–17] While there are a large number of reports describing different methods for successfully combining exogenous species into MOFs,[18–21] the encapsulation of nanoparticles is particularly promising due to the innovative functional properties that cannot be obtained from the parent MOFs alone.[22–26] Typically, the encapsulation of nanoparticles is achieved through the introduction of precursors using solution impregnation, gas-phase infiltration or a solid-phase method, and subsequent conversion into the corresponding functional components inside the frameworks.[27–29] However, in this two-step approach, free nanoparticles are often present which need to be removed from the system. This is generally achieved by a gravimetric separation step, exploiting the different sedimentation rate between the nanoparticles and the MOF crystals, before separating the magnetic composite from the pure MOF.[25] Additionally, particle size and morphology are limited by the cavities of the MOFs.[30,31] Moreover, the framework can potentially be degraded during nanoparticle formation.[30,31]

In an attempt to overcome this difficulty, approaches for the growth of MOFs around pre-formed functional particles have been successfully proposed.[32,33] These approaches involve the addition of preformed functional species into the MOF precursor solution and the subsequent *in situ* formation of MOF crystals with embedded functional particles. Furthermore, it has been demonstrated that the heterospecies can

[a] *Division of Materials Science & Engineering, Graduate School of Engineering, Osaka Prefecture University, 1-1 Gakuen-cho, Naka-ku, Sakai, Osaka 599-8531, Japan. E-mail: matsumac@chem.osakafu-u.ac.jp*
[b] *Institute for Catalysis, Hokkaido University, N-21, W-10, Sapporo 001-0021, Japan*
[c] *CSIRO Manufacturing, Private Bag 10, Clayton South, Victoria 3169, Australia. E-mail: paolo.falcaro@tugraz.at*
[d] *Department of Materials Science and Engineering, Monash University, Clayton, Victoria, 3168, Australia*
[e] *Graz University of Technology, Institute of Physical and Theoretical Chemistry, Stremayrgasse 9/Z2, 8010 Graz, Austria*

† Electronic supplementary information (ESI) available: SEM, TEM, FTIR, XRD, XANES, FT-EXAFS, and TGA analyses on ceramics and MOFs, catalytic tests on deacetalization and Knoevenagel condensation reactions, and reusability test on hydrogenation reaction. See DOI: 10.1039/c7ce00390k

improve the kinetics of MOF formation,[34–36] as nano- and micro-particles can act as crystallization facilitators promoting faster MOF growth. On the other hand, functional nanoparticles tend to aggregate under the acidic environment created by the dissociation of ligands during this solution process.[37,38] Therefore, surface modification and the choice of the proper solvent can help the nucleation and growth of the MOFs around the functional components.[39,40] An interesting emerging approach that overcomes this issue involves the use of ceramic materials as the metal source for the direct conversion into a MOF composite.[41–44] Interestingly, the ceramic materials can act as protecting agents for functional nanoparticles reducing their exposure to harsh conditions.[41–44] Furthermore, the use of ceramics as precursors has allowed mild conditions to be used (*e.g.* water/alcohol at room temperature) with short processing times.[45]

Here we describe a simple approach to incorporate magnetic nanoparticles into MOFs by taking advantage of the method developed in our previous study, as shown in Fig. 1.[46] We previously reported the synthesis of HKUST-1 (also called $Cu_3(BTC)_2$, BTC = 1,3,5-benzenetricarboxylate) through conversion from Cu-based ceramic precursors ($Cu_2(OH)_3NO_3$) at room temperature as an ideal method for the permanent localization[46] of the corresponding MOF. In this study, Fe_3O_4 magnetic nanoparticles have been embedded into the Cu-based ceramic material used as a precursor for the synthesis of repositionable[46] HKUST-1 crystals. The Fe_3O_4@$Cu_2(OH)_3NO_3$ composite was subsequently converted to Fe_3O_4-incorporated HKUST-1 (Fe_3O_4@HKUST-1) through exposure to an alcoholic solution containing 1,3,5-benzenetricarboxylic acid (H_3BTC). The conversion of the ceramic into MOFs can be performed at room temperature. The obtained Fe_3O_4@HKUST-1 has been successfully separated from the HKUST-1 thanks to magnetic localization using a commercial magnet, that enabled the composite to be isolated and removed from the pure MOF crystals.[25] With the same approach, the material has been utilized as an easily recyclable heterogeneous catalyst for a one-pot cascade reaction. Moreover, Pd nanoparticles have also been embedded into the HKUST-1 material, to prepare a novel advanced composite based on different nanoparticles encapsulated within the same MOF (*i.e.* Pd/Fe_3O_4@HKUST-1). The composite Pd/Fe_3O_4@HKUST-1 was found to be an active catalyst for the hydrogenation of olefin. Thanks to the magnetic component that confers dynamic localization properties, the composite showed promising recyclability properties. The method proposed here can offer a simple one-step approach to incorporate different functional nanoparticles into the same MOF particle.

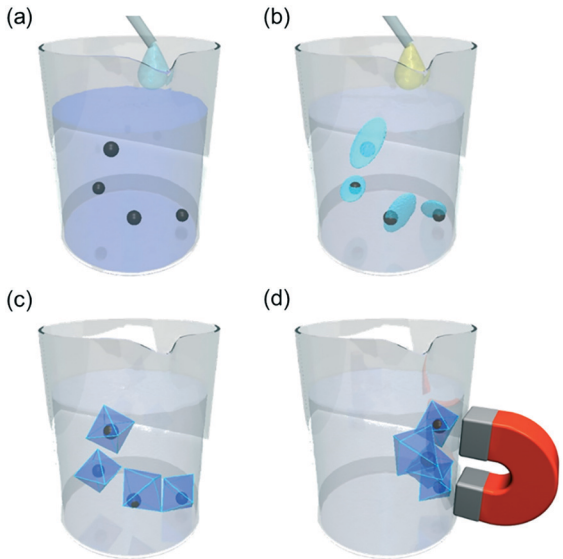

Fig. 1 Schematic illustrations showing the integration of Fe_3O_4 nanoparticles into HKUST-1 through conversion from a composite of a Cu-based ceramic material and Fe_3O_4 (Fe_3O_4@$Cu_2(OH)_3NO_3$). (a) Fe_3O_4@$Cu_2(OH)_3NO_3$ is obtained by adding aq. NH_3 into water containing $Cu(NO_3)_2{\cdot}3H_2O$ and Fe_3O_4. (b and c) Fe_3O_4@$Cu_2(OH)_3NO_3$ is converted into HKUST-1 material by adding a mixed solution of EtOH and water containing H_3BTC at room temperature for 10 min. (d) The prepared composite (Fe_3O_4@HKUST-1) is collected by immobilizing the composite crystals with a magnet.

Results and discussion

Characterization of materials

Fe_3O_4@$Cu_2(OH)_3NO_3$ was prepared from $Cu(NO_3)_2{\cdot}3H_2O$ and Fe_3O_4 by exposure to ammonia. $Cu_2(OH)_3NO_3$ was also prepared for comparison without adding Fe_3O_4 nanoparticles. Using scanning electron microscopy (SEM), plate-like structures were observed for both Fe_3O_4@$Cu_2(OH)_3NO_3$ and $Cu_2(OH)_3NO_3$ samples, as shown in Fig. 2a and c. Subsequently, the conversion of both samples was carried out by

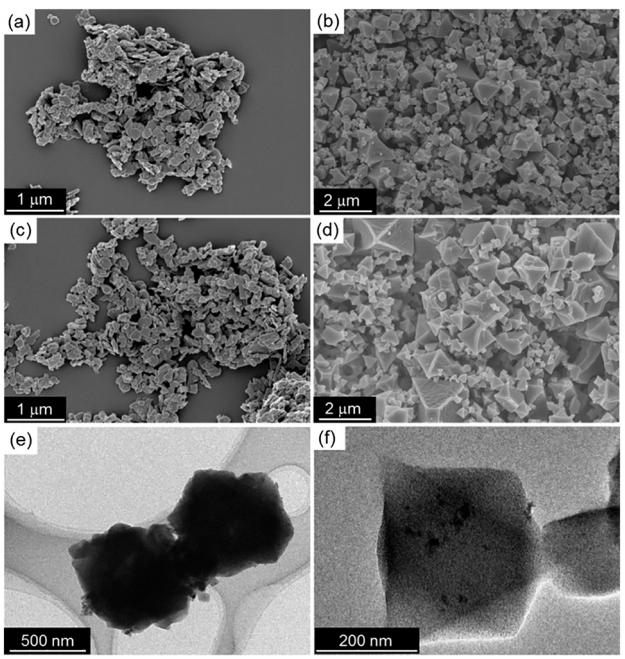

Fig. 2 SEM images of (a) Fe_3O_4@$Cu_2(OH)_3NO_3$, (b) Fe_3O_4@HKUST-1, (c) $Cu_2(OH)_3NO_3$ and (d) HKUST-1. (e and f) TEM images of Fe_3O_4@HKUST-1.

adding a mixed solution of ethanol (EtOH) and water containing H_3BTC. After about 10 seconds of reaction time, the color change of the precursor materials from light blue to deep turquoise could be detected visibly, thus indicating the formation of HKUST-1.[47] Significant changes in morphology from the Cu-based precursors to the octahedral crystals of HKUST-1 were observed after 10 min of the conversion time (Fig. 2b and d). SEM images at 10 s and 1 min conversion time were also obtained to follow the evolution of the HKUST-1 (see Fig. S1 in the ESI†). The octahedral morphology of the particles suggests the successful formation of HKUST-1 crystals.[47] It should be noted that the particle size of the Fe_3O_4@HKUST-1 composite is smaller than that of HKUST-1 without Fe_3O_4 nanoparticles. This change in crystal size can be attributed to the Fe_3O_4 nanoparticles acting as seeding materials and/or crystallization modulators for the formation of HKUST-1 crystals.[34–37] Inductively coupled plasma optical emission spectroscopy (ICP-OES) analysis was performed to determine the loading amount of Fe. The results revealed 1.57 wt% of Fe in the Fe_3O_4@HKUST-1 composite. Transmission electronic microscope (TEM) observations were also made to investigate Fe_3O_4 nanoparticles in Fe_3O_4@HKUST-1, as given in Fig. 2e and f. The TEM images demonstrate that Fe_3O_4@HKUST-1 contains Fe_3O_4 nanoparticles with an average diameter of 24 nm. The observed particle size matches well with the previous report describing preparation of the Fe_3O_4 nanoparticles.[48] These results suggest that Fe_3O_4 nanoparticles remained essentially unchanged even after the conversion process and integrated in HKUST-1.

Powder X-ray diffraction (XRD) measurements were carried out in order to ascertain the formation of HKUST-1 crystals, as shown in Fig. 3a. After the conversion to MOF, the measured diffraction patterns matched with previously-reported HKUST-1 diffraction patterns.[47] Interestingly, no diffraction peaks corresponding to residual precursors or oxide species were observed in the patterns. Peaks from the Fe_3O_4 nanoparticles were not observed because of the low loading amount. FT-IR measurements were also performed to characterize the Fe_3O_4@$Cu_2(OH)_3NO_3$ and Fe_3O_4@HKUST-1 (Fig. S2†). In the spectra for Fe_3O_4@$Cu_2(OH)_3NO_3$, a wide band attributed to O–H stretching modes was observed in the region of 3550–3200 cm^{-1}.[49] The absorption bands at around 877, 1044, 1240, 1296, 1333 and 1416 cm^{-1} were assigned to vibrational modes of nitrate (NO_3^-) ions having an interaction with copper hydroxide layers.[50,51] The remaining bands at 670 and 772 cm^{-1} were assigned to the Cu–OH stretching mode.[52] After treatments with an alcoholic solution containing H_3BTC, the intensity of the absorption bands attributed to O–H stretching modes in the region of 3550–3200 cm^{-1} decreased significantly. New modes were observed and assigned to the organic molecules used as ligands in the HKUST-1 frameworks (BTC); 729, 760, 940 cm^{-1}: C–CO_2 stretching, 1114 cm^{-1}: C–O stretching, 1373, 1449, 1645 cm^{-1}: COO–Cu_2 stretching.[53–55] These results confirm the successful conversion of the precursor ceramic to HKUST-1. It was also found that the absorption band coming from nitrate ions was present in the Fe_3O_4@HKUST-1 sample. Thermogravimetric analysis (TGA) curves of Fe_3O_4@HKUST-1 exhibited weight loss at around 300 °C which is attributable to the framework decomposition while Fe_3O_4@$Cu_2(OH)_3NO_3$ showed weight loss at around 250 °C (Fig. S3†). This result supports the formation of HKUST-1 from the ceramic precursor. It was also observed that Fe_3O_4@HKUST-1 and HKUST-1 showed an almost identical profile, suggesting that incorporation of Fe_3O_4 in the framework did not affect the thermal stability of the framework material.

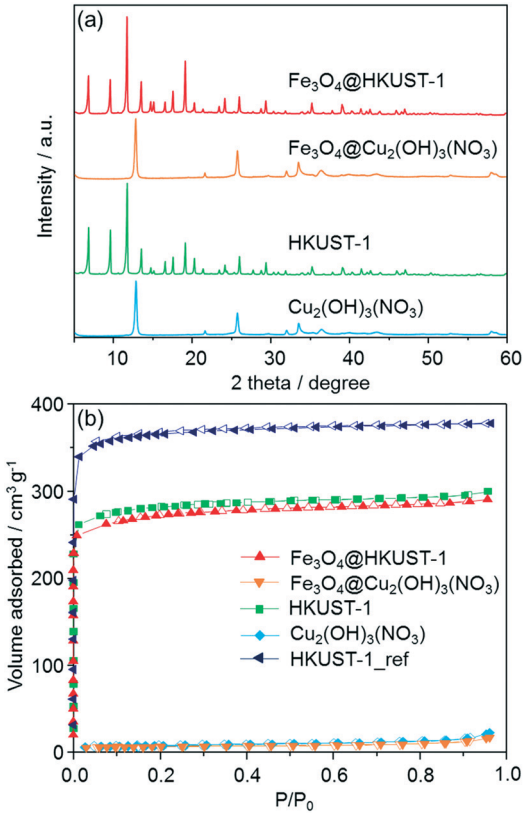

Fig. 3 (a) XRD patterns of Fe_3O_4@HKUST-1, Fe_3O_4@$Cu_2(OH)_3NO_3$, HKUST-1 and $Cu_2(OH)_3NO_3$. The peaks from Fe_3O_4 nanoparticles cannot be seen in the diffraction patterns of Fe_3O_4@HKUST-1 and Fe_3O_4@$Cu_2(OH)_3NO_3$, most likely due to the low loading amount; (b) N_2 adsorption isotherms of Fe_3O_4@$Cu_2(OH)_3NO_3$, Fe_3O_4@HKUST-1, $Cu_2(OH)_3NO_3$, HKUST-1 and HKUST-1_ref measured at 77 K. Closed and open symbols represent adsorption and desorption isotherms, respectively.

N_2 adsorption isotherms are shown in Fig. 3b. Using the BET (Brunauer–Emmett–Teller) method, the specific surface areas of Fe_3O_4@$Cu_2(OH)_3NO_3$ and $Cu_2(OH)_3NO_3$ were measured to be 19 and 23 $m^2\ g^{-1}$ respectively, demonstrating that the feedstock ceramic materials have low accessible surface area. After conversion into the MOF, type I isotherms were measured for both Fe_3O_4@HKUST-1 and HKUST-1, indicating a different microporosity. The specific surface areas of Fe_3O_4@HKUST-1 and HKUST-1 were determined to be 952 and 986 $m^2\ g^{-1}$, respectively. HKUST-1_ref, synthesized using the conventional aqueous room temperature protocol

proposed by Bradshaw *et al.*,[56] was found to have the surface area of 1236 m^2 g^{-1}. The surface areas of the HKUST-1 materials prepared using the method proposed here were found to be c.a. 20% lower than that of HKUST-1_ref. This result suggests the residual precursor species still exist in the framework, which is consistent with the results obtained by FT-IR measurements. This conclusion is supported by previous studies into converting other Cu-based ceramics into HKUST-1.[45,46,57]

In order to gain further insights into the growth of the HKUST-1 crystals, *in situ* small-angle X-ray scattering (SAXS) and wide-angle X-ray scattering (WAXS) measurements were conducted at the Australian Synchrotron. For these measurements, the Cu-based precursor materials were placed in a capillary with the mixed solution of EtOH and water, followed by the controlled addition of the alcoholic solution containing the H_3BTC linker using a syringe. Once filled with the solution, the capillary was illuminated by a high-intensity X-ray beam, and the scattered radiation was collected by the two 2D detectors. The obtained 2D scattering patterns have been background-subtracted, radially integrated and plotted as a function of the reaction time. The obtained SAXS/WAXS-based diffraction patterns for the conversion of Fe_3O_4@$Cu_2(OH)_3NO_3$ and $Cu_2(OH)_3NO_3$ are shown in Fig. 4. For the conversion of Fe_3O_4@$Cu_2(OH)_3NO_3$ into Fe_3O_4@HKUST-1, the peaks attributed to the HKUST-1 structure appeared just after the ligand was injected (within 10 seconds). Within 50 seconds, plateaus were found in the intensities of the peaks corresponding to HKUST-1, including two intense peaks that appeared at Q = 0.67 and 0.82 $Å^{-1}$ arising from the (022) and (222) planes of the HKUST-1 framework, respectively. This result indicates that the conversion process stopped approximately 50 seconds after the injection of the ligand into the capillary containing Fe_3O_4@$Cu_2(OH)_3NO_3$ nanopowders. In comparison, the kinetics of the conversion of $Cu_2(OH)_3NO_3$ into HKUST-1 was slightly slower than that with Fe_3O_4 nanoparticles and plateaus were found to occur approximately 90 seconds after the injection of the ligand. This suggests that the Fe_3O_4 nanoparticles induce a faster conversion of the $Cu_2(OH)_3NO_3$ precursor into HKUST-1. This could be explained by the role of Fe_3O_4 nanoparticles as crystallization facilitators to promote faster MOF growth relative to the absence of nanoparticles.[34–37]

The local structure of Fe species in Fe_3O_4@HKUST-1 was investigated by Fe K-edge XAFS (XANES and EXAFS) measurements (Fig. 5a and b). The edge position as well as the shape of the XANES spectrum of Fe_3O_4@HKUST-1 correspond well to those of Fe_3O_4 used as a reference. Fourier transform of the EXAFS (FT-EXAFS) spectrum (without phase-shift corrections) of Fe_3O_4@HKUST-1 exhibits two strong peaks corresponding to the Fe–O shell (1.0–2.0 Å) and the Fe–Fe shell (2.5–3.5 Å) which can be seen in the reference Fe_3O_4 spectrum.[58,59] These results indicate that the Fe species in

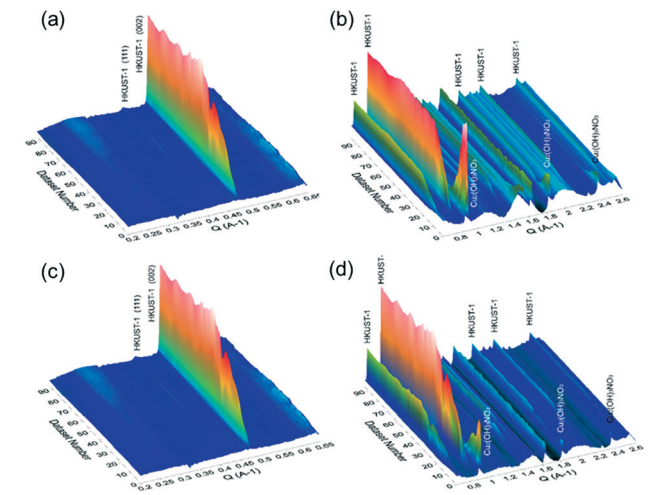

Fig. 4 Time series of radially averaged SAXS (a and c) and WAXS (b and d) data. The nucleation and growth of Fe_3O_4@HKUST-1 (a and b) and HKUST-1 (c and d) at room temperature is observed when the alcoholic solution containing H_3BTC is added to the solution containing Cu-based precursors. Dataset number corresponds to SAXS/WAXS images were collected every 3.15 s. The ligand was injected at t = 30 s (dataset 10).

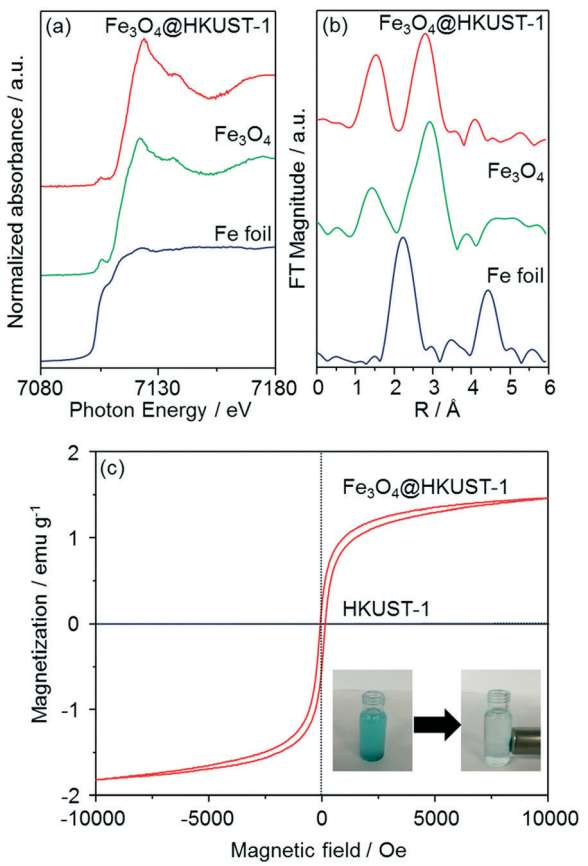

Fig. 5 Fe K-edge (a) XANES and (b) FT-EXAFS spectra of Fe_3O_4, Fe_3O_4@HKUST-1 and Fe metallic foil. (c) Magnetization curves of Fe_3O_4@HKUST-1 and HKUST-1, and photographs of Fe_3O_4@HKUST-1 collected by a magnet. The magnetization measurements were performed at 300 K.

Fe_3O_4@HKUST-1 exist as Fe_3O_4 without change during the conversion process.

The magnetic properties of Fe_3O_4@HKUST-1 were measured by a vibrating sample magnetometer with an applied field to investigate the ability of the composite to be used as a recyclable catalyst. Fig. 5c illustrates the room-temperature magnetization curves of Fe_3O_4@HKUST-1 and HKUST-1 without Fe_3O_4 nanoparticles. Unlike HKUST-1, Fe_3O_4@HKUST-1 displayed small hysteresis loops, suggesting that the incorporated Fe_3O_4 is ferromagnetic.[60,61] We also demonstrated that Fe_3O_4@HKUST-1 is attracted to a magnet (inset of Fig. 5c) and, as a result, it can be easily separated after use as a heterogeneous catalyst.

Catalytic study (one-pot reaction)

Potential catalytic properties of Fe_3O_4@HKUST-1 were investigated through a one-pot sequential cascade reaction. One-pot reactions have drawn much attention as an attractive synthetic concept for improving overall process efficiency and reducing production wastes.[62–66] Among them, we performed a sequential deacetalization–Knoevenagel condensation reaction. It is well-known that deacetalization reactions are catalysed by Brønsted acidic sites[67,68] and Knoevenagel condensation reactions are catalysed by base sites.[69,70] Also, Knoevenagel condensation reactions are catalysed by Lewis acid.[71] Since MOFs contain Brønsted acidic sites and Lewis acidic sites due to carboxylic acid moieties (–COOH groups) and coordinatively unsaturated metal sites,[72–75] HKUST-1 is, in principle, a suitable candidate for one-pot sequential cascade. To further investigate the potential of HKUST-1 as a catalyst, deacetalization and Knoevenagel condensation were individually performed and the catalytic activities of Fe_3O_4@HKUST-1 were tested. Fig. S4† shows the results of deacetalization of benzaldehyde dimethylacetal and Knoevenagel condensation of benzaldehyde with malononitrile. In the presence of Fe_3O_4@HKUST-1, the reaction efficiently proceeded to give benzaldehyde. Moreover, it was found from the inspection of the time course for Knoevenagel condensation shown in Fig. S5b† that Fe_3O_4@HKUST-1 also catalyzed the reaction, producing the corresponding benzylidene–malononitrile from benzaldehyde and malononitrile. These findings suggest that Fe_3O_4@HKUST-1 possesses both Brønsted acidic and Lewis acidic sites to produce benzylidene–malononitrile *via* two-step deacetalization and Knoevenagel condensation process.

Next, Fe_3O_4@HKUST-1 was applied to one-pot sequential deacetalization and Knoevenagel condensation from benzaldehyde dimethylacetal and malononitrile to produce benzylidenemalononitrile. The reaction was carried out at 363 K using 1,4-dioxane as a solvent. Fig. 6 shows time course of the one-pot reaction. Benzylidenemalononitrile (3, square) was efficiently generated from benzaldehyde dimethylacetal (1, circle) *via* a pathway involving the initial formation of benzaldehyde (2, diamond), and that the yield of 3 reached 99% after a 5 h reaction time. It was also confirmed that the reaction did not take place in the absence of a catalyst (entry 11 in Table 1). For comparison purposes, other materials including conventional catalysts were applied for this one-pot reaction. The results are summarized in Table 1. The reaction was hardly promoted over Fe_3O_4 (entry 2), indicating that HKUST-1 played an important role in the progression of the reaction. While Fe_3O_4@HKUST-1 gave 99% of the final product, HKUST-1 made from $Cu_2(OH)_3NO_3$ without Fe_3O_4 and HKUST-1_ref made by the conventional method gave 94% and 67% yields, respectively. This difference in the catalytic activity could be explained by taking into account the different particle size of the materials (See Fig. 2 and Fig. S5 in the ESI† for the particle size of HKUST-1_ref). Since HKUST-1 is a microporous material with ~1 nm-size

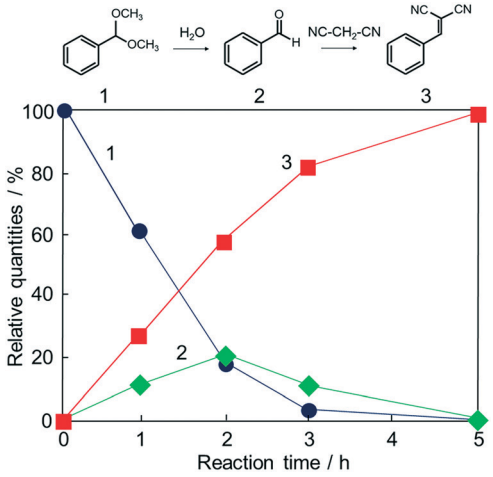

Fig. 6 Time course of the one-pot deacetalization–Knoevenagel condensation reaction over Fe_3O_4@HKUST-1; benzaldehyde dimethylacetal (1, ●), benzaldehyde (2, ◆), benzylidenemalononitrile (3, ■).

Table 1 One-pot sequential deacetalization and Knoevenagel condensation reaction using various catalysts[a]

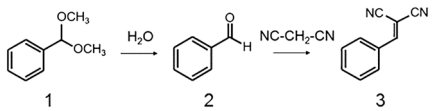

Entry	Catalyst	Conversion (%)	Yield (%) 2	Yield (%) 3
1	Fe_3O_4@HKUST-1	100	1	99
2	Fe_3O_4	13	7	6
3	HKUST-1	100	6	94
4	HKUST-1_ref	77	10	67
5	Fe_3O_4@$Cu_2(OH)_3NO_3$	19	5	14
6	$Cu(NO_3)_2{\cdot}3H_2O$	42	15	27
7	H_3BTC	14	10	2
8	MgO	33	15	18
9	Al_2O_3	38	16	22
10	SiO_2	8	4	4
11	No catalyst	2	0	2

[a] Reaction conditions: benzaldehyde dimethylacetal (1 mmol), malononitrile (3 mmol), 1,4-dioxane (4 mL), catalyst (50 mg), 363 K, 5 h.

channels,[47] which can restrict facile substrate diffusion within the particles, a catalyst with smaller particle size is thought to have more easily accessible surface area and better substrate diffusion.[76] Additionally, by synthesizing the MOF from the ceramic material, a higher density of coordinatively unsaturated metal sites (defect sites) can be expected. The combination of the two causes would explain the high catalytic activity compared to HKUST-1 without Fe_3O_4 and HKUST-1_ref. Fe_3O_4@$Cu_2(OH)_3NO_3$ as well as $Cu(NO_3)_2{\cdot}3H_2O$ and H_3BTC lead to only low yields under the same condition. The use of conventional heterogeneous catalysts such as MgO, Al_2O_3 and SiO_2 showed reduced performance relative to Fe_3O_4@HKUST-1. These results demonstrate that Fe_3O_4@HKUST-1 served as an effective bifunctional catalyst for the sequential deacetalization and Knoevenagel condensation reaction.

Subsequently, recyclability tests using Fe_3O_4@HKUST-1 were performed. After a 5 h reaction, the Fe_3O_4@HKUST-1 catalyst was collected using a magnet, washed with 1,4-dioxane, dried at 313 K in air and then reused for the next catalytic test. As shown in Fig. 7a, Fe_3O_4@HKUST-1 could be reused at least 5 times with the retention of high catalytic activity and selectivity. The stability of Fe_3O_4@HKUST-1 was investigated by XRD measurements before and after the reaction (Fig. 7b). The diffraction pattern corresponding to the HKUST-1 structure was maintained after the reaction, indicating that Fe_3O_4@HKUST-1 possesses good resistance to degradation during one-pot reaction cascades. Furthermore, a leaching test was performed, as shown in Fig. S6.† Specifically, we observed that removal of the catalyst following a 1 h period caused the reaction to cease, indicating that the catalyst has heterogeneous nature.

Catalytic study (hydrogenation of olefin)

To further exploit the versatility of the current magnetic MOF nanocomposite, Pd nanoparticles were added into the solution containing Fe_3O_4@$Cu_2(OH)_3NO_3$, then the conversion into MOF was promoted with the addition of the linker solution. The formation of HKUST-1 was confirmed by XRD analysis (Fig. S7†) performed on the magnetically collected and washed powders. An ICP-OES analysis was carried out to determine the loading amount of Pd. The result revealed that the magnetic composite contained 0.32 wt% of Pd. In order to clarify the state of Pd in the material, XAFS measurements were performed and are shown in Fig. S8.† The edge position and the shape of the XANES spectrum of Pd/Fe_3O_4@HKUST-1 are similar to those of the Pd metallic foil used as a reference. The FT-EXAFS spectrum (without phase-shift corrections) of the magnetic composite shows one peak corresponding to neighbouring Pd atoms (2.0–3.0 Å). Other peaks arising from potential Pd oxides were not observed in the spectrum. These data indicate that Pd species in Pd/Fe_3O_4@HKUST-1 system mainly exist in a metal state without a significant change during the conversion process. The composite was investigated using TEM to further confirm the presence of Pd particles in the material (Fig. S9†). The results clearly show 10–20 nm Pd nanoparticles located within the material. The prepared Pd/Fe_3O_4@HKUST-1 composite has been utilized for hydrogenation reaction of 1-octene to octane in the liquid phase. While no reaction occurred when using Fe_3O_4@HKUST-1, the presence of Pd/Fe_3O_4@HKUST-1 successfully produced octane from 1-octene.

Fig. 8 shows the time course of the reaction. The yield of octane was 98% within 3 h reaction time. These results indicate that Pd nanoparticles act as an effective catalyst for this hydrogenation reaction while the pure Fe_3O_4@HKUST-1 does not show appreciable catalytic activity. In order to check the reusability and stability of Pd/Fe_3O_4@HKUST-1, recycling tests and XRD measurements were performed (Fig. S10†). Pd/Fe_3O_4@HKUST-1 could be recycled at least 5 times without significant activity loss. Moreover, XRD patterns of the catalyst did not significantly change after the catalytic reaction. As in the sequential deacetalization–Knoevenagel condensation reaction, a leaching test further confirmed that there is no contribution from the leached species (Fig. S11†). Furtheremore, ICP-OES analysis was carried out for the reaction solution after the reaction using Pd/Fe_3O_4@HKUST-1. The obtained result showed that Pd and Fe species in the solution were below the detection limit (*ca.* 10 ppm). These results indicate the durability of the Pd/Fe_3O_4@HKUST-1 as a multifunctional material for catalytic applications. However,

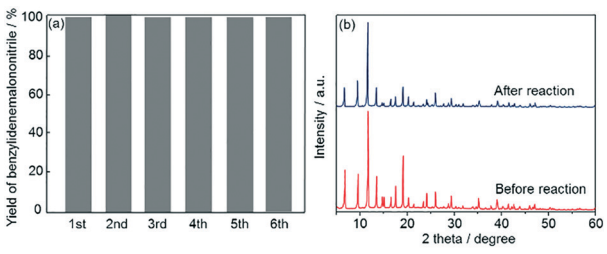

Fig. 7 (a) Reusability study of Fe_3O_4@HKUST-1 for the one-pot deacetalization–Knoevenagel condensation reaction. (b) XRD patterns of Fe_3O_4@HKUST-1 before and after the catalytic reaction.

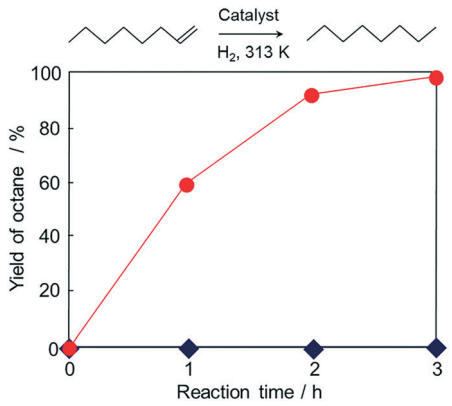

Fig. 8 Time course of hydrogenation of 1-octene over Pd/Fe_3O_4@HKUST-1 (●) and Fe_3O_4@HKUST-1 (◆).

it should be noted here that slight morphological change in the catalysts might be caused during the reactions and this could influence the catalytic activity and selectivity[77,78] although such changes in the catalysis were not observed for the reactions employed in this study. Compared to previous studies describing the synthesis of complex MOF composites prepared by multistep processes,[79,80] the novel conversion method developed in this study is facile and enables the incorporation of different functional nanoparticles, without significant changes[81,82] or the need for elaborate structures.[79,80,83]

Experimental details

Materials and methods

Ethanol (EtOH), $Cu(NO_3)_2{\cdot}3H_2O$, $FeSO_4{\cdot}7H_2O$ and 1,3,5-benzenetricarboxylic acid (H3BTC) were purchased from Acros Organics. Citric acid was obtained from Aldrich Chemical Co. 30% aq. Ammonia was provided by Chem-Supply. 1,4-Dioxane, NaOH, $PdCl_2$, polyvinylpyrrolidone (PVP) K30 and $NaBH_4$ were supplied by Nacalai Tesque Inc. Benzaldehyde dimethylacetal, benzaldehyde, malononitrile, 1-octene and *n*-decane were purchased from Tokyo Chemical Industry Co., Ltd. MgO was obtained from Kishida Chemical Co., Ltd. Al_2O_3 was purchased from Evonik. All materials were used as received without purification.

Materials preparation

Fe_3O_4 nanoparticles were prepared according to the method provided by Hui and co-workers.[48] In a typical procedure, NaOH (1.60 g, 40.0 mmol) is dissolved, under magnetic stirring, in 190 mL of water, in a 250 mL round-bottomed single-neck flask. Subsequently, $NaNO_3$ (0.170 g, 2.00 mmol) and $Na_3C_6H_5O_7{\cdot}2H_2O$ (2.94 g, 10.0 mmol) are added and the mixture heated to 100 °C for 1 h. In another container, $FeSO_4{\cdot}7H_2O$ (5.56 g, 20.0 mmol) is dissolved in 10.0 mL of deionized water using an ultrasound bath. The iron(II) solution is added at once into the hydroxide/citrate solution under vigorous stirring (>500 rpm), and the mixture turns to dark brown in few seconds. The flask is kept stirring at 100 °C for an additional hour, then the stirbar removed, and the mixture let to cool down naturally. The magnetic nanoparticles are collected using a commercial N45 magnet, and the supernatant discarded. The magnetic nanoparticles are placed in another vessel and suspended in 100 mL of deionized water, using an ultrasound bath, for 30 min. The material is collected again as described above, and this washing procedure is repeated 3 times. At the end, the magnetic nanoparticles are shaken in 100 mL of acetone, then dried in a rotary evaporator. This water-stripping procedure is repeated twice, then the obtained brown to black material is dried in a vacuum oven (<30 mbar) at 60 °C for at least 3 h. The prepared sample is denoted as $Fe_3O_4@Cu_2(OH)_3NO_3$.

Fe_3O_4@HKUST-1 was prepared from $Fe_3O4@Cu_2(OH)_3NO_3$ as follows: $Fe_3O_4@Cu_2(OH)_3NO_3$ (97 mg) was added to the mixed solution of 5 mL of EtOH and 2 mL of water containing H_3BTC (106 mg) as organic linker. The mixture was stirred for 10 min at room temperature. Then, crystals were separated from the Fe_3O_4@HKUST-1 composite by the localization of the magnetically responsive composite with a commercial magnet. The resulting powder was washed with water and EtOH, and then collected *via* centrifugation at 5000 rpm. The collected samples were dried under vacuum.

Pd nanoparticles were prepared by a modified version of the previously reported procedure proposed by Hou and co-workers.[84] Typically, $PdCl_2$ (20 mg), PVP (834 mg), and 20 mL of H_2O were mixed and stirred at 0 °C in an ice bath. A mixture of $NaBH_4$ (30 mg) and 0.5 mL of H_2O was then added in the above solution, which was stirred for 30 min.

Pd/Fe_3O_4@HKUST-1 was prepared similarly to the synthesis of Fe_3O_4@HKUST-1 by adding colloidal Pd nanoparticles. $Fe_3O4@Cu_2(OH)_3NO_3$ (97 mg) and 5 mL of the above Pd colloidal solution were added to the mixed solution of 5 mL of EtOH and 2 mL of water containing H_3BTC (106 mg) as the organic linker. The mixture was stirred for 10 min at room temperature. Then, the magnetic framework composite crystals were isolated from the pure crystals not containing Fe_3O_4 particles by magnetic collection. The resulting powder was washed with water and EtOH, and then collected *via* centrifugation at 5000 rpm. The collected samples were dried under vacuum.

General methods

The surface morphologies of samples were observed using a field emission scanning electron microscope (FE-SEM; Merlin; Carl Zeiss Germany) with a thin iridium film coating. Standard θ–2θ X-ray diffraction (XRD) data were recorded on a Rigaku Smart Lab diffractometer using Cu Kα radiation (λ = 1.5406 Å). Inductively coupled plasma optical emission spectroscopy (ICP-OES) was performed by using Varian 730-ES axial ICP-OES. Nitrogen adsorption–desorption isotherms were collected using a BEL-SORP mini (BEL Japan, Inc.) at 77 K. Fourier transform infrared spectroscopy (FT-IR: ALPHA FT-IR spectrometer, Bruker Optik GmbH) was employed in the ATR configuration. Thermogravimetric analysis (TGA) was carried out using a thermal analyzer (Shimadzu DTG-60), with a heating rate of 10 K min^{-1} in air. Small-angle X-ray scattering (SAXS) and wide-angle X-ray scattering (WAXS) were performed at the Australian Synchrotron. A capillary with a 1.5 mm diameter was used for the *in situ* characterization by SAXS and WAXS. Once filled with the solution, the capillary was illuminated by a high-intensity X-ray beam at the beamline, and the scattered radiation was collected by the detector (Pilatus 1 M). An on-axis video camera allowed for parallax free sample viewing and alignment at all times before and during exposure, enabling precise and rapid sample alignment. Transmission electron microscope (TEM) images were recorded using a JEM-2000FX operating under a 200 kV accelerating voltage. XAFS (XANES and EXAFS) spectra were recorded at the BL-01B1 facility of SPring-8 at the Japan Synchrotron Radiation Research Institute (JASRI). Fe K-edge and Pd K-edge XAFS spectra were recorded in the

fluorescence mode using a Si(111) double-crystal monochromator at room temperature. Magnetization curves were recorded using a vibrating sample magnetometer (VSM, Riken Denshi Co., Ltd., BHV-50H).

Catalytic study

One-pot deacetalization–Knoevenagel condensation reaction was carried out in a 35 mL glass reactor. A solution of benzaldehyde dimethylacetal (1 mmol), malononitrile (5 mmol) and 4 mL of 1,4-dioxane was stirred at 90 °C with 50 mg of the catalysts in powder form. The progression of the reaction was monitored using gas chromatography (Shimadzu GC-14B with a flame ionization detector) equipped with an InertCap®1 capillary column.

Reusability of the catalyst was studied as follows. After the first run, the catalyst was collected by a magnet, washed three times with 1,4-dioxane, dried at 40 °C in air and reused for the next run. The above procedure was repeated five times.

The hydrogenation of 1-octene was performed to evaluate the catalytic activity of Pd/Fe_3O_4@HKUST-1. The catalysts (50 mg), 1-octene (5 mmol), and 10 mL of methanol were introduced into a glass reaction vessel with a reflux condenser. The resulting mixture was bubbled with hydrogen for 15 min and then stirred at 40 °C under hydrogen bubbling (10 mL min^{-1}). The progress of the reaction was monitored by gas chromatography analysis using an internal standard technique (*n*-decane).

Conclusions

Magnetic Fe_3O_4 nanoparticles have been successfully incorporated into HKUST-1 through the conversion of a Cu-based ceramic precursor. Fe_3O_4 played a significant role in the conversion process from ceramic to HKUST-1 with an influence on the kinetics (faster) and the MOF particle size (smaller). It was also revealed by several characterization techniques that the magnetic Fe_3O_4 particles were incorporated into HKUST-1 without causing significant aggregation. The prepared material (Fe_3O_4@HKUST-1) has been successfully utilized as a magnetically recyclable heterogeneous catalyst to promote one-pot sequential deacetalization–Knoevenagel condensation reaction. In addition, the results showed that Fe_3O_4/HKUST-1 exhibits higher catalytic activities than conventional inorganic heterogeneous catalysts (*e.g.* Al_2O_3, SiO_2, MgO). Pd nanoparticles were also incorporated alongside Fe_3O_4 within HKUST-1 and successfully used for the hydrogenation of 1-octene in the liquid phase. These findings suggest new possibilities for the encapsulation of different nanoparticles within MOFs demonstrating that multifunctional catalysts can be obtained through the conversion from ceramic composites into MOF composites.

Acknowledgements

The present work is supported by "ACCEL Project" from the Japan Science and Technology Agency, by Grants-in-Aid for Scientific Research from the Ministry of Education, Culture, Sports, Science and Technology of Japan (No. 25410241 and 15K17903) and Strategic Young Researcher Overseas Visits Program for Accelerating Brain Circulation. Part of this research was undertaken on the SAXS/WAXS beamline at the Australian Synchrotron, Melbourne, Victoria, Australia with the support of Dr. Nigel Kirby and Dr. Adrian Hawley. X-ray absorption measurements were performed at the BL-01B1 facility of SPring-8 at the Japan Synchrotron Radiation Research Institute (JASRI) (No. 2014B1279).

References

1 S. Furukawa, J. Reboul, S. Diring, K. Sumida and S. Kitagawa, *Chem. Soc. Rev.*, 2014, **43**, 5700–5734.
2 H. Furukawa, K. E. Cordova, M. O'Keeffe and O. M. Yaghi, *Science*, 2013, **341**, 1230444.
3 G. Férey, *Chem. Soc. Rev.*, 2007, **37**, 191–214.
4 O. M. Yaghi, M. O'Keeffe, N. W. Ockwig, H. K. Chae, M. Eddaoudi and J. Kim, *Nature*, 2003, **423**, 705–714.
5 M. Eddaoudi, J. Kim, N. Rosi, D. Vodak, J. Wachter, M. O'Keeffe and O. M. Yaghi, *Science*, 2002, **295**, 469–472.
6 V. Guillerm, D. Kim, J. F. Eubank, R. Luebke, X. Liu, K. Adil, M. S. Lah and M. Eddaoudi, *Chem. Soc. Rev.*, 2014, **43**, 6141–6172.
7 K. Liang, R. Ricco, J. Reboul, S. Furukawa and P. Falcaro, in *The Sol-Gel Handbook*, ed. D. Levy and M. Zayat, Wiley-VCH Verlag GmbH & Co. KGaA, Weinheim, Germany, 2015, pp. 471–486.
8 J. D. Evans, C. J. Sumby and C. J. Doonan, *Chem. Soc. Rev.*, 2014, **43**, 5933–5951.
9 S. Ou and C.-D. Wu, *Inorg. Chem. Front.*, 2014, **1**, 721–734.
10 D. Bradshaw, A. Garai and J. Huo, *Chem. Soc. Rev.*, 2012, **41**, 2344–2381.
11 A. Aijaz, A. Karkamkar, Y. J. Choi, N. Tsumori, E. Rönnebro, T. Autrey, H. Shioyama and Q. Xu, *J. Am. Chem. Soc.*, 2012, **134**, 13926–13929.
12 J. Lee, O. K. Farha, J. Roberts, K. A. Scheidt, S. T. Nguyen and J. T. Hupp, *Chem. Soc. Rev.*, 2009, **38**, 1450–1459.
13 M. L. Foo, R. Matsuda and S. Kitagawa, *Chem. Mater.*, 2014, **26**, 310–322.
14 K. Liang, R. Ricco, C. M. Doherty, M. J. Styles, S. Bell, N. Kirby, S. Mudie, D. Haylock, A. J. Hill, C. J. Doonan and P. Falcaro, *Nat. Commun.*, 2015, **6**, 7240.
15 T. Toyao, M. Saito, S. Dohshi, K. Mochizuki, M. Iwata, H. Higashimura, Y. Horiuchi and M. Matsuoka, *Res. Chem. Intermed.*, 2016, **42**, 7679–7688.
16 P. Falcaro, R. Ricco, A. Yazdi, I. Imaz, S. Furukawa, D. Maspoch, R. Ameloot, J. D. Evans and C. J. Doonan, *Coord. Chem. Rev.*, 2016, **307**, 237–254.
17 C. M. Doherty, E. Knystautas, D. Buso, L. Villanova, K. Konstas, A. J. Hill, M. Takahashi and P. Falcaro, *J. Mater. Chem.*, 2012, **22**, 11470–11474.

18 P. Falcaro, R. Ricco, C. M. Doherty, K. Liang, A. J. Hill and M. J. Styles, *Chem. Soc. Rev.*, 2014, **43**, 5513–5560.
19 M. Kim, J. F. Cahill, Y. Su, K. A. Prather and S. M. Cohen, *Chem. Sci.*, 2012, **3**, 126–130.
20 P. Falcaro and S. Furukawa, *Angew. Chem., Int. Ed.*, 2012, **51**, 8431–8433.
21 C. J. Doonan, W. Morris, H. Furukawa and O. M. Yaghi, *J. Am. Chem. Soc.*, 2009, **131**, 9492–9493.
22 Y. Liu and Z. Tang, *Adv. Mater.*, 2013, **25**, 5819–5825.
23 W. Zhang, G. Lu, S. Li, Y. Liu, H. Xu, C. Cui, W. Yan, Y. Yang and F. Huo, *Chem. Commun.*, 2014, **50**, 4296–4298.
24 H. Zhang, S. Qi, X. Niu, J. Hu, C. Ren, H. Chen and X. Chen, *Catal. Sci. Technol.*, 2014, **4**, 3013–3024.
25 R. Ricco, L. Malfatti, M. Takahashi, A. J. Hill and P. Falcaro, *J. Mater. Chem. A*, 2013, **1**, 13033–13045.
26 P. Falcaro, F. Normandin, M. Takahashi, P. Scopece, H. Amenitsch, S. Costacurta, C. M. Doherty, J. S. Laird, M. D. H. Lay, F. Lisi, A. J. Hill and D. Buso, *Adv. Mater.*, 2011, **23**, 3901–3906.
27 M. Meilikhov, K. Yusenko, D. Esken, S. Turner, G. Van Tendeloo and R. A. Fischer, *Eur. J. Inorg. Chem.*, 2010, **2010**, 3701–3714.
28 M. Müller, S. Hermes, K. Kähler, M. W. E. van den Berg, M. Muhler and R. A. Fischer, *Chem. Mater.*, 2008, **20**, 4576–4587.
29 H.-L. Jiang, T. Akita, T. Ishida, M. Haruta and Q. Xu, *J. Am. Chem. Soc.*, 2011, **133**, 1304–1306.
30 C. Rösler and R. A. Fischer, *CrystEngComm*, 2015, **17**, 199–217.
31 G. Li, H. Kobayashi, K. Kusada, J. M. Taylor, Y. Kubota, K. Kato, M. Takata, T. Yamamoto, S. Matsumura and H. Kitagawa, *Chem. Commun.*, 2014, **50**, 13750–13753.
32 G. Lu, S. Li, Z. Guo, O. K. Farha, B. G. Hauser, X. Qi, Y. Wang, X. Wang, S. Han, X. Liu, J. S. DuChene, H. Zhang, Q. Zhang, X. Chen, J. Ma, S. C. J. Loo, W. D. Wei, Y. Yang, J. T. Hupp and F. Huo, *Nat. Chem.*, 2012, **4**, 310–316.
33 K. Sugikawa, Y. Furukawa and K. Sada, *Chem. Mater.*, 2011, **23**, 3132–3134.
34 C. M. Doherty, D. Buso, A. J. Hill, S. Furukawa, S. Kitagawa and P. Falcaro, *Acc. Chem. Res.*, 2014, **47**, 396–405.
35 D. Buso, K. M. Nairn, M. Gimona, A. J. Hill and P. Falcaro, *Chem. Mater.*, 2011, **23**, 929–934.
36 D. Buso, A. J. Hill, T. Colson, H. J. Whitfield, A. Patelli, P. Scopece, C. M. Doherty and P. Falcaro, *Cryst. Growth Des.*, 2011, **11**, 5268–5274.
37 K. Sugikawa, S. Nagata, Y. Furukawa, K. Kokado and K. Sada, *Chem. Mater.*, 2013, **25**, 2565–2570.
38 T. Tsuruoka, H. Kawasaki, H. Nawafune and K. Akamatsu, *ACS Appl. Mater. Interfaces*, 2011, **3**, 3788–3791.
39 Y. Abdollahian, J. L. Hauser, I. R. Colinas, C. Agustin, A. S. Ichimura and S. R. J. Oliver, *Cryst. Growth Des.*, 2014, **14**, 1506–1509.
40 P. Falcaro, A. J. Hill, K. M. Nairn, J. Jasieniak, J. I. Mardel, T. J. Bastow, S. C. Mayo, M. Gimona, D. Gomez, H. J. Whitfield, R. Riccò, A. Patelli, B. Marmiroli, H. Amenitsch, T. Colson, L. Villanova and D. Buso, *Nat. Commun.*, 2011, **2**, 237.
41 Y. Mao, J. Li, W. Cao, Y. Ying, P. Hu, Y. Liu, L. Sun, H. Wang, C. Jin and X. Peng, *Nat. Commun.*, 2014, **5**, 5532.
42 Y. Liu, W. Zhang, S. Li, C. Cui, J. Wu, H. Chen and F. Huo, *Chem. Mater.*, 2014, **26**, 1119–1125.
43 J. Reboul, S. Furukawa, N. Horike, M. Tsotsalas, K. Hirai, H. Uehara, M. Kondo, N. Louvain, O. Sakata and S. Kitagawa, *Nat. Mater.*, 2012, **11**, 717–723.
44 J. Reboul, K. Yoshida, S. Furukawa and S. Kitagawa, *CrystEngComm*, 2014, **17**, 323–330.
45 G. Majano and J. Pérez-Ramírez, *Adv. Mater.*, 2013, **25**, 1052–1057.
46 T. Toyao, K. Liang, K. Okada, R. Ricco, M. J. Styles, Y. Tokudome, Y. Horiuchi, A. J. Hill, M. Takahashi, M. Matsuoka and P. Falcaro, *Inorg. Chem. Front.*, 2015, **2**, 434–441.
47 S. S.-Y. Chui, S. M.-F. Lo, J. P. H. Charmant, A. G. Orpen and I. D. Williams, *Science*, 1999, **283**, 1148–1150.
48 C. Hui, C. Shen, T. Yang, L. Bao, J. Tian, H. Ding, C. Li and H.-J. Gao, *J. Phys. Chem. C*, 2008, **112**, 11336–11339.
49 I. Y. Park, K. Kuroda and C. Kato, *Solid State Ionics*, 1990, **42**, 197–203.
50 G. Socrates, *Infrared and Raman characteristic group frequencies: tables and charts*, Wiley, Chichester, 3rd edn, 2010, as paperback.
51 K. Nakamoto, *Infrared and Raman spectra of inorganic and coordination compounds*, Wiley, Hoboken, N.J, 6th edn, 2009.
52 A. Yin, X. Guo, W.-L. Dai and K. Fan, *J. Phys. Chem. C*, 2009, **113**, 11003–11013.
53 J. L. C. Rowsell and O. M. Yaghi, *J. Am. Chem. Soc.*, 2006, **128**, 1304–1315.
54 S. Loera-Serna, L. L. Núñez, J. Flores, R. López-Simeon and H. I. Beltrán, *RSC Adv.*, 2013, **3**, 10962–10972.
55 S. Loera-Serna, M. A. Oliver-Tolentino, M. de Lourdes López-Núñez, A. Santana-Cruz, A. Guzmán-Vargas, R. Cabrera-Sierra, H. I. Beltrán and J. Flores, *J. Alloys Compd.*, 2012, **540**, 113–120.
56 J. Huo, M. Brightwell, S. El Hankari, A. Garai and D. Bradshaw, *J. Mater. Chem. A*, 2013, **1**, 15220–15223.
57 K. Okada, R. Ricco, Y. Tokudome, M. J. Styles, A. J. Hill, M. Takahashi and P. Falcaro, *Adv. Funct. Mater.*, 2014, **24**, 1969–1977.
58 L. Signorini, L. Pasquini, L. Savini, R. Carboni, F. Boscherini, E. Bonetti, A. Giglia, M. Pedio, N. Mahne and S. Nannarone, *Phys. Rev. B: Condens. Matter Mater. Phys.*, 2003, **68**, 195423.
59 G. Subías, J. García and J. Blasco, *Phys. Rev. B: Condens. Matter Mater. Phys.*, 2005, **71**, 155103.
60 T. Yang, C. Shen, Z. Li, H. Zhang, C. Xiao, S. Chen, Z. Xu, D. Shi, J. Li and H. Gao, *J. Phys. Chem. B*, 2005, **109**, 23233–23236.
61 Z. L. Liu, Y. J. Liu, K. L. Yao, Z. H. Ding, J. Tao and X. Wang, *J. Mater. Synth. Process.*, 2002, **10**, 83–87.
62 K. Motokura, M. Tada and Y. Iwasawa, *J. Am. Chem. Soc.*, 2009, **131**, 7944–7945.
63 S. Shylesh, A. Wagener, A. Seifert, S. Ernst and W. R. Thiel, *Angew. Chem., Int. Ed.*, 2010, **49**, 184–187.

64 M. Sasidharan, S. Fujita, M. Ohashi, Y. Goto, K. Nakashima and S. Inagaki, *Chem. Commun.*, 2011, **47**, 10422–10424.
65 A. Corma, T. Ródenas and M. J. Sabater, *J. Catal.*, 2011, **279**, 319–327.
66 T. Toyao, M. Saito, Y. Horiuchi and M. Matsuoka, *Catal. Sci. Technol.*, 2014, **4**, 625–628.
67 R. A. Duval, R. L. Allmon and J. R. Lever, *J. Med. Chem.*, 2007, **50**, 2144–2156.
68 F. Douelle, A. S. Capes and M. F. Greaney, *Org. Lett.*, 2007, **9**, 1931–1934.
69 S. Hasegawa, S. Horike, R. Matsuda, S. Furukawa, K. Mochizuki, Y. Kinoshita and S. Kitagawa, *J. Am. Chem. Soc.*, 2007, **129**, 2607–2614.
70 Y. Horiuchi, T. Toyao, M. Fujiwaki, S. Dohshi, T.-H. Kim and M. Matsuoka, *RSC Adv.*, 2015, **5**, 24687–24690.
71 M. J. Climent, A. Corma, S. Iborra and A. Velty, *J. Mol. Catal. A: Chem.*, 2002, **182–183**, 327–342.
72 M. Opanasenko, A. Dhakshinamoorthy, M. Shamzhy, P. Nachtigall, M. Horáček, H. Garcia and J. Čejka, *Catal. Sci. Technol.*, 2013, 500–507.
73 L. Mitchell, B. Gonzalez-Santiago, J. P. S. Mowat, M. E. Gunn, P. Williamson, N. Acerbi, M. L. Clarke and P. A. Wright, *Catal. Sci. Technol.*, 2013, **3**, 606–617.
74 R. Ameloot, F. Vermoortele, J. Hofkens, F. C. De Schryver, D. E. De Vos and M. B. J. Roeffaers, *Angew. Chem., Int. Ed.*, 2013, **52**, 401–405.
75 T. Toyao, M. Fujiwaki, Y. Horiuchi and M. Matsuoka, *RSC Adv.*, 2013, **3**, 21582–21587.
76 T. Kiyonaga, M. Higuchi, T. Kajiwara, Y. Takashima, J. Duan, K. Nagashima and S. Kitagawa, *Chem. Commun.*, 2015, **51**, 2728–2730.
77 D. Loffreda, D. Simon and P. Sautet, *J. Catal.*, 2003, **213**, 211–225.
78 F. Calle-Vallejo, D. Loffreda, M. T. M. Koper and P. Sautet, *Nat. Chem.*, 2015, **7**, 403–410.
79 J.-M. Yan, Z.-L. Wang, L. Gu, S.-J. Li, H.-L. Wang, W.-T. Zheng and Q. Jiang, *Adv. Energy Mater.*, 2015, **5**, 1500107.
80 F. Ke, L. Wang and J. Zhu, *Nanoscale*, 2015, **7**, 1201–1208.
81 M. Zhang, Y. Yang, C. Li, Q. Liu, C. T. Williams and C. Liang, *Catal. Sci. Technol.*, 2014, **4**, 329–332.
82 L. Chen, H. Chen and Y. Li, *Chem. Commun.*, 2014, **50**, 14752–14755.
83 L. Lin, T. Zhang, H. Liu, J. Qiu and X. Zhang, *Nanoscale*, 2015, **7**, 7615–7623.
84 W. Hou, N. Dehm and R. Scott, *J. Catal.*, 2008, **253**, 22–27.

